International Journal of Refrigeration 100 (2019) 368–379

Contents lists available at ScienceDirect

International Journal of Refrigeration

journal homepage: www.elsevier.com/locate/ijrefrig

An analytical design tool for sorber bed heat exchangers of sorption cooling systems

Hesam Bahrehmand, Majid Bahrami*

Laboratory for Alternative Energy Conversion (LAEC), School of Mechatronic Systems Engineering, Simon Fraser University, 250-13450 102 Avenue, Surrey, BC V3T 0A3, Canada

ARTICLE INFO

Article history:
Received 4 November 2018
Revised 31 January 2019
Accepted 1 February 2019
Available online 6 February 2019

Keywords:
Sorption cooling systems
Heat and mass transfer
Analytical modeling
Optimization
Specific cooling power
Coefficient of performance

ABSTRACT

A new 2-D analytical solution is presented and validated using the data collected from our custom-built gravimetric large pressure jump test bed and two-sorber bed sorption test bed. The proposed closed-form 2-D transient solution includes all salient thermophysical and sorption properties, heat exchanger geometry, and operational conditions as well as the thermal contact resistance at the interface in sorber beds. It is shown that the optimum amount of thermally conductive additive in the sorbent depends on the geometrical and heat transfer characteristics of the sorber bed and the cycle time. Furthermore, it is shown that the sorber bed geometry, heat transfer characteristics, sorption composite composition and cycle time can have conflicting effects on specific cooling power and coefficient of performance and should be optimized simultaneously to establish an optimal design.

Outil de conception analytique pour les échangeurs de chaleur à lit à sorption des systèmes de refroidissement à sorption

Mots-clés: Système de refroidissement à sorption; Transfert de chaleur et de masse; Modélisation analytique; Optimisation; Puissance de refroidissement spécifique; Coefficient de performance

1. Introduction

Conventional air conditioning (A/C) systems use vapor compression refrigeration (VCR) technology, which consumes significant amount of electricity, generated mainly from burning fossil fuels. Almost 15% of the electricity produced globally is used by A/C and refrigeration units (Building Energy Data Book, 2012; Askalany et al., 2013; Pridasawas, 2006). According to Natural Resources Canada (NRCan), VCR systems in vehicles A/C increase fuel consumption by up to 20% because of the extra load on the engine (nrcan, 2018). Further, the commonly used refrigerants in VCR systems, hydrofluorocarbons (HFCs), contribute to climate change due to their tremendous greenhouse gas effects. Therefore, using alternative refrigerants with low global warming potential (GWP) and low ozone depletion potential (ODP) offer substantial environmental benefit over HFCs. A promising alternative to the conventional VCR system is sorption cooling system (SCS) – featuring refrigerants with low GWP and ODP – in which sorber beds replace the compressor and low-grade thermal energy is used to regenerate the sorber beds (Pan et al., 2016, 2018; Pan and Wang, 2017a, 2017b).

However, the following main technical challenges impede the widespread commercialization of SCS (Wu et al., 2009; Zhao et al., 2012; Sharafian et al., 2015; Hu et al., 1997): (i) low specific cooling power (SCP), resulting from the poor heat, and thus mass transfer in sorber beds, due to low sorbent thermal diffusivity and unoptimized heat exchanger design; and (ii) low coefficient of performance (COP) compared to VCR, partially due to the high thermal inertia of the sorber bed heat exchangers (HEX). In addition, conventional SCS operate in vacuum pressures which make them prone to leaks which in turn lead to degradation of power and frequent maintenance. These issues result in heavier,

* Corresponding author.
E-mail addresses: sbahrehm@sfu.ca (H. Bahrehmand), mbahrami@sfu.ca (M. Bahrami).

https://doi.org/10.1016/j.ijrefrig.2019.02.003
0140-7007/

Nomenclature

A	heat transfer area, m^2
b	height of fin and sorbent (m)
Bi	Biot number
c	specific heat capacity, J kg^{-1} K^{-1}
Fo	Fourier number
h	convective heat transfer coefficient (W m^{-2} K^{-1})
h_{ads}	enthalpy of adsorption, J kg^{-1}
h_{fg}	enthalpy of evaporation, J kg^{-1}
H	height, m
k	thermal conductivity, W m^{-1} K^{-1}
L	characteristic length
m'	slope of fitted line for uptake versus temperature, $\omega = m'T + b$ (−0.01 for sorption and −0.0092 for desorption) (Bahrehmand et al., 2018a, 2018b)
p	pressure, Pa
p_0	saturation pressure, Pa
Q	energy, J
R	thermal resistance, K m^2 W^{-1}
T	temperature, K
t	time (s), thickness (m)
u	velocity, m s^{-1}
$\dot{V}$	volumetric flow rate, m^3 s^{-1}
W	width of the tube cross-section (m)
X	spatial eigenfunction in x, η direction
x	coordinate
y	coordinate

Greek symbols

α	thermal diffusivity, m^2 s^{-1}
γ	eigenvalue in η direction
Γ	temporal Eigenfunction
η	dimensionless coordinate of x
θ	dimensionless temperature
η	dimensionless coordinate
κ	dimensionless thermal conductivity ratio
λ	eigenvalue in ξ direction
Λ	dimensionless thermal contact conductance
μ	dimensionless thermal diffusivity ratio
ξ	dimensionless coordinate of y
ρ	density, kg m^{-3}
τ	cycle time, s
φ	graphite flake content in the sorbent (g graphite flake g^{-1} total sorbent)
ψ	spatial eigenfunction in y, ξ direction
ω	sorbate uptake (g H_2O g^{-1} dry sorbent)

Subscripts

0	initial condition
ads	adsorption
c	channel
cond	condenser
des	desorption
evap	evaporator/evaporative
eq	equilibrium
f	fin
fs	fin spacing
g	gas or vapor
htf	heat transfer fluid
s	sorbent
sorb	sorbent
sorp	sorption
t	tube
w	water

Abbreviations

COP	coefficient of performance
HEX	heat exchanger
G-LPJ	gravimetric large pressure jump
SCP	specific cooling power
TCR	thermal contact resistance
TCS	temperature control system

bulkier, and costlier SCS compared to VCR systems. To address these issues, sorber bed HEX, which includes the sorbent, HEX and the heat transfer fluid, need to be specifically designed and optimized for SCS. In this paper, we propose a new 2-D analytical model that can be used as a platform for design and optimization of finned tube sorber beds of SCS.

Many researchers have developed thermodynamic, lumped, numerical and analytical models of sorber beds to enhance and optimize the performance of SCS. A summary of available studies in the literature is presented in Table 1. However, one can conclude that the literature lacks an accurate model that includes heat exchanger geometrical features, salient thermophysical and sorption properties as well as operational input parameters and: (i) considers the transient behavior of sorber beds; (ii) thermal contact resistance at the interface between the sorption material and the HEX; and (iii) yields a closed-form solution, which is particularly important for multi-domain optimization of sorber beds, where a large number of parameters should be considered simultaneously in the design analysis.

The present model is developed to address these challenges and is validated against experimental data collected from our custom-designed gravimetric large pressure jump (G-LPJ) test bed and two-sorber bed sorption test bed in our lab.

To improve the thermal diffusivity of the sorbent material, we prepared a consolidated composite, consisting of $CaCl_2$, silica gel B150, with added natural graphite flakes. The added thermally conductive graphite flakes reduce the active sorbent fraction in the composite creating a need for establishing an optimum composition for each application, more details can be found in our previous study (Bahrehmand et al., 2018c). Using the validated closed-form solution, a parametric study is conducted to investigate the effect of important parameters, i.e., HEX geometry, heat transfer characteristics, and cycle time on SCS performance. The proposed analytical solution enables determining optimized values for: (i) fin thickness, (ii) fin height, (iii) sorbent thickness, (iv) fluid channel height, (v) the amount of thermally-conductive additive in the composite sorbent, and (vi) cycle time in SCS.

2. Model development

Finned-tube heat exchanger (HEX) is selected as the sorber bed type due to its relatively high SCP and COP (Sharafian and Bahrami, 2014). The solution domain of the HEX, shown in Fig. 1(a), can be used to predict the performance of the entire sorber bed. An optimized sorber bed has been designed based on the present model and is being tested, the results will be published in our future study to not make this paper too long; a picture of the sorber bed is presented in Fig. 1(b).

The following is the list of the assumptions used in the development of the present model:

- The heat transfer fluid is assumed to have a constant temperature along the solution domain; justifiable due to the relatively higher heat capacity of the heat transfer fluid (Wu et al., 2009).
- The boundaries of the sorbent and the fin, which are in contact with low-pressure refrigerant vapor, are assumed adiabatic. This is a fair hypothesis since the Biot number is low as shown

Table 1
Summary of the available modeling approaches of the sorber beds of SCS.

Modeling approach	Ref.	Characteristics of the parametric study	Merits	Limitations
Thermodynamic model	(Tamainot-Telto et al., 2009), (Henninger et al., 2012)	• Driving temperature	• Very low computation time	• Predicts only the upper performance limits
Lumped model	(Pan and Wang, 2018)	• Cycle time	• Low computation time	• Uniform sorbent temperature
	(Ahmed and Al-Dadah, 2012)	• Fin spacing • Cycle time		• Uniform sorption of refrigerant • Neglects inter-particle heat and mass transfer resistances
	(Saha et al., 2007)	• Generation temperature lift		
	(Rogala, 2017)	• Fin height • Fin spacing		• Dependent on previous time steps
Steady state analytical lumped model	(Verde et al., 2017)	• Flat tube thickness • Fin pitch • Fin thickness • Water channel wall thickness	• Very low computation time	• Neglects transient behavior of system • Neglects inter-particle heat and mass transfer resistances
1-D transient analytical model	(Jeric and Nottage, 1967)		• Low computation time	• Unable to consider 2-D sorber bed and HEX geometry
	(Bahrehmand et al., 2018a, 2018b)	• Sorbent thermal diffusivity • HEX thermal diffusivity • Thermal contact resistance • HEX to sorbent thickness ratio	• Considers 1-D spatial and temporal variation of sorbent temperature and sorbate uptake	
Numerical model	(El Fadar, 2015)	• Fin spacing • Number of fins	• Considers spatial and temporal variation of sorbent temperature and sorbate uptake	• High computation time • Dependent on previous time steps
	(Hong et al., 2015)	• Fin pitch • Fin thickness • Fin height • Diffusion coefficient • Particle size • Cycle time • Cycle ratio • Hot water temperature • Fluid velocity • Porosity		
	(Çağlar, 2016)	• Fin radius • Fin thickness • Number of fins		
	(Solmus et al., 2012)	• Adsorbent bed thickness • Convective heat transfer coefficient • Sorbent thermal conductivity		
	(Li et al., 2004)	• Fin spacing • Fin height		
	(Mohammed et al., 2017)	• Particle diameter • Adsorbent bed thickness		
	(Niazmand and Dabzadeh, 2012; Niazmand et al., 2012; Mahdavikhah and Niazmand, 2013; Mohammadzadeh Kowsari et al., 2018; Golparvar et al., 2018)	• Fin height • Fin spacing • Particle diameter		
Present 2-D transient analytical model		• Graphite flake content in the sorbent • Fin height • Fin thickness • Sorbent thickness • Fluid channel height • Cycle time	• Low computation time • Considers 2-D spatial and temporal variation of sorbent temperature and sorbate uptake • Independent of previous time steps • Considers anisotropic thermal conductivity • Considers TCR at the interface between sorbent and fin	

Note: References El Fadar (2015), Hong et al. (2015), Li et al. (2004) and Niazmand et al. (2012) consider the thermal contact resistance at the interface between the sorbent and the HEX.

below:

$$h(T_{vapor}-T_s)=k_s\frac{\partial T_s}{\partial y}\Rightarrow O(Bi_y)=O\left(\frac{ht_s}{k_s}\right)=\frac{0.5\times0.001}{0.3}=0.0017$$
$$h(T_{vapor}-T_s)=k_s\frac{\partial T_s}{\partial x}\Rightarrow O(Bi_x)=O\left(\frac{hb}{k_s}\right)=\frac{0.5\times0.01}{0.3}=0.017$$
$$h\left(T_{vapor}-T_f\right)=k_f\frac{\partial T_f}{\partial x}\Rightarrow O\left(Bi_{x,f}\right)=O\left(\frac{hb}{k_f}\right)=\frac{0.5\times0.01}{236.5}=2.11e-5 \quad (1)$$

where, h is the convective heat transfer coefficient between the water vapor (the refrigerant) and the sorbent (Zhao et al., 2012; Wakao and Kaguei, 1982). It was shown by Wakao and Kaguei (1982) that the interfacial convection and the external convection are of the same order of magnitude. Also, the radiative heat transfer is negligible because of low temperature difference between the sorbent and its surrounding (10–20 K).

- Thermophysical properties of the sorbent and HEX are assumed constant. Averaged values over the range of operating conditions are used (Table 2).
- The convection term in the energy equation, which accounts for the sorbate convection inside the sorbent coating, is assumed negligible as the Peclet number, which represents the ratio of the convection to the diffusion term in the energy equation, is

Table 2
Graphite flake content in the sorbent, thermophysical properties, geometrical specifications, and SCS cycle parameters used for the baseline case and model validation.

	Baseline case			Validation with two-sorber bed sorption test bed				Validation with G-LPJ test bed		
	Sorbent	Al fin	Al tube	Sorbent		Al fin	Copper tube	Sorbent	Graphite Fin	Copper tube
ϕ (wt%)	10	–	–	0	20	–	–	0–20	–	–
ρ (kg/m^3)	665	2699	2699	654	675	2699	8932		1550	8932
c (J/kgK)	1082	909	909	1004	1120	909	386		748	386
α (m^2/s)	4.1e−7	9.6e−	9.6e−5	2.3e−7	1.3e−6	9.6e−5	1.1e−4		α_x= 2.5e−04 α_y= 4.3e−06	1.1e−4
h_{ads} (J/kg)	2.77e6	–	–	2.77e6		–	–	2.77e6	–	–
t (mm)	2	2	1	1.12		0.15	1.55	5	1.7	1.5
b, H_c, W_c, and D (cm)	b=2	b=2	H_c=0.6 W_c=1.3	b=1.24		b=1.24	D=1.65	b=3.5	b=3.5	H_c=0.5 W_c=4
τ (min)	15			In Fig. 6				In Fig. 5		
$\dot{V}$(L/min)	5									
$TCR{\cdot}A$ (K m^2/W)	0.0019 (Bahrehmand et al., 2018a)									

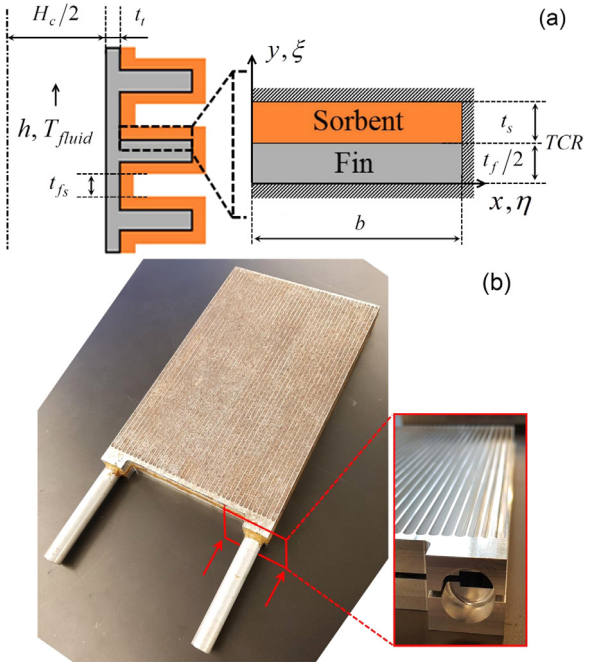

Fig. 1. (a) The solution domain for finned-tube sorber bed heat exchangers and (b) a finned flat tube sorber bed.

small as follows (Wu et al., 2009).

$$O(Pe) = O\left(\frac{\rho_g c_{p,g} u_g L}{k_s}\right) = \frac{10^{-2} \times 10^{3} \times 10^{-1} \times 10^{-3}}{10^{-1}} = 0.01 \tag{2}$$

where, L is the characteristic length and in the order of millimeters and u_g, vapor velocity, is in the order of 0.1 m/s (Mahdavikhah and Niazmand, 2013). Also, ρ_g and $c_{p,g}$ are density and specific heat of water vapor, and are equal to 0.051 kg/m^3 and 1904 J/kg, respectively.

- The sorbent coated on the tube in the gap between the sorbent coatings on the fins, i.e. t_{fs} shown in Fig. 1, is neglected as t_{fs} is much smaller than the fin height.

Using the above-mentioned assumptions, the energy equation for the sorbent layer and the fin in Cartesian coordinates can be written as follows.

$$\frac{\partial T_i}{\partial t} = \alpha_{i,x}\frac{\partial^2 T_i}{\partial x^2} + \alpha_{i,y}\frac{\partial^2 T_i}{\partial y^2} + \frac{1}{(\rho c_p)_i} G_i(t)$$
$$T_i(x, y, t)$$
$$i = s, f \tag{3}$$

$$G_i(t) = \begin{cases} \rho_s h_{ads}\frac{d\omega}{dt}, & i = s \\ 0, & i = f \end{cases} \tag{4}$$

where, $i = s, f$ represents the sorbent and fin domains, respectively. The convective boundary conditions are:

$$\frac{1}{R_s}\left(T_s(0, y, t) - T_{fluid}\right) = k_s\frac{\partial T_s(0, y, t)}{\partial x} \tag{5}$$

$$\frac{1}{R_f}\left(T_f(0, y, t) - T_{fluid}\right) = k_{f,x}\frac{\partial T_f(0, y, t)}{\partial x} \tag{6}$$

$$R_s = \frac{t_t}{k_{f,x}} + \frac{1}{h} + TCR \cdot A \quad \left(\frac{K\,m^2}{W}\right) \tag{7}$$

$$R_f = \frac{t_t}{k_{f,x}} + \frac{1}{h} \quad \left(\frac{K\,m^2}{W}\right) \tag{8}$$

where, the convective heat transfer coefficient is calculated by the correlation proposed by Gnielinski (1976) as follows.

$$h = 0.012\frac{k_w}{2H_c}\left(\mathrm{Re}^{0.87} - 280\right)\mathrm{Pr}^{0.4} \tag{9}$$

The adiabatic boundary conditions are:

$$\frac{\partial T(b, y, t)}{\partial x} = 0 \tag{10}$$

$$\frac{\partial T_s(x, t_s + t_f, t)}{\partial y} = 0 \tag{11}$$

Due to symmetry, one can write the following for the lower side of the fin:

$$\frac{\partial T_f(x, 0, t)}{\partial y} = 0 \tag{12}$$

Thermal contact resistance (TCR) between the sorbent and the HEX surface is important and can be up to 28% of the total thermal resistance inside a sorber bed (Bahrehmand et al., 2018a; Sharafian et al., 2014; Rezk et al., 2013). Hence, it is included in the present model, as a parameter with a constant value. Continuity of heat flux as well as temperature jump/drop created by TCR are considered at the interface between the sorbent coating and fin as follows.

$$k_{f,y}\frac{\partial T_f(x, t_f, t)}{\partial y} = k_s\frac{\partial T_s(x, t_f, t)}{\partial y} \tag{13}$$

$$-k_{f,y}\frac{\partial T_f(x, t_f, t)}{\partial y} = \frac{1}{TCR \cdot A}\left(T_f(x, t_f, t) - T_s(x, t_f, t)\right) \tag{14}$$

The dimensionless energy equation, Eqs. (A1)–(A11), is solved using Eigenfunction Expansion Method. Eigenfunction Expansion

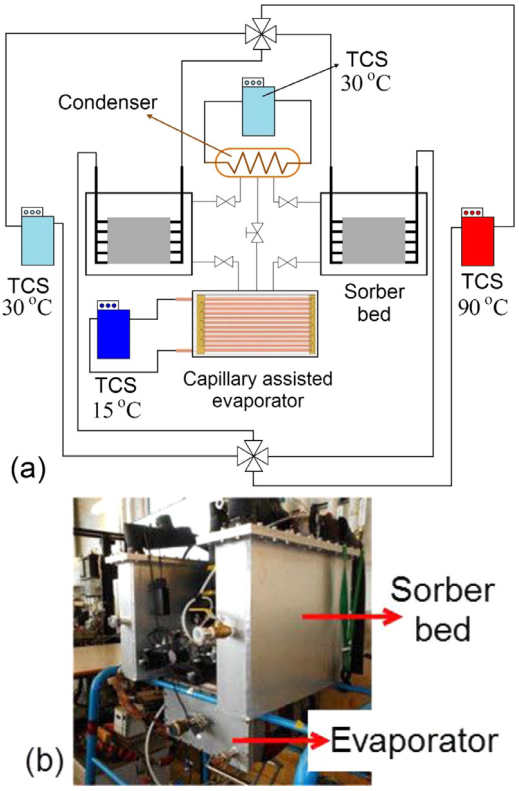

Fig. 2. (a) Schematic and (b) a picture of the 2-sorber bed sorption test bed, TCS: temperature control system.

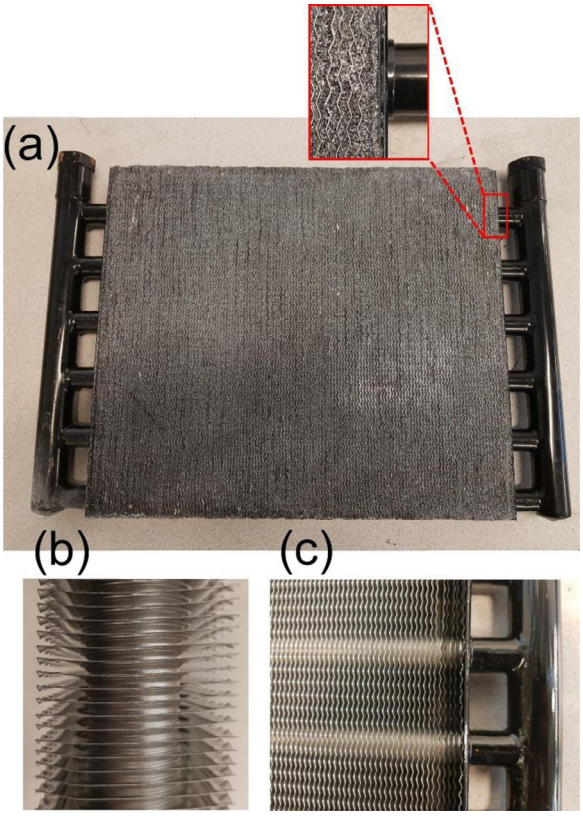

Fig. 3. (a) Sorber bed coated with the composite sorbent, $CaCl_2$, silica gel, PVA and graphite flakes, and the finned-tube HEX without sorbent coating (b) top view and (c) front view.

Method has been widely used in heat transfer problems, particularly for multi-layer domains, time-dependent boundary conditions and/or source terms (Singh et al., 2016; Moghadam, 2015; Julius et al., 2017; Biswas and Singh, 2017; Weng et al., 1983; Fakoor-Pakdaman et al., 2015). The methodology of the solution is presented in Appendix A. A code is developed in MATLAB to calculate the eigenvalues and eigenfunctions in η and ξ (non-dimensional) coordinates as well as Gamma function as a function of Fourier number (dimensionless time). The closed-form of the dimensionless transient 2-D temperature domain is found in a series form as follows.

$$\theta(\eta,\xi,Fo)=\sum_{n=1}^{\infty}\sum_{m=1}^{\infty}X_n(\eta)\psi_{nm}(\xi)\Gamma_{nm}(Fo) \tag{15}$$

Our study indicates that the first 2 terms in eigenfunction X ($n=1$ and 2) and one term in eigenfunction ψ ($m=1$) yield the accuracy of 99% in the temperature distribution calculation. Each run takes about 1.5 min on a 3.4 GHz PC.

A relationship is obtained between the water uptake and sorbent temperature for each isobaric sorption and desorption process in large temperature jump and large pressure jump tests in Appendix B.

3. Experimental study: two-sorber bed sorption test bed

A custom-built test bed available in our lab is used to validate the proposed model. Fig. 2 shows a schematic and a picture of the two-sorber bed sorption test bed. A custom-designed capillary-assisted evaporator and a helical coil shell and tube HEX were used as the evaporator and the condenser, respectively. The sorber beds and the evaporator were placed inside custom-built vacuum chambers. Check valves were installed between the sorber beds and the condenser and gate valves were installed between the evaporator and the beds. A needle valve with high precision flow adjustment (Speedivalve SP16K, Edwards) and a U-tube were installed between the condenser and the evaporator. The whole system was vacuumed for 6 h before the tests. Two temperature control systems were used to keep the evaporator at 15 °C and the condenser at 30 °C. Furthermore, two temperature control systems were set to 90 °C and 30 °C for desorption and adsorption processes, respectively. Two four-way valves were employed to switch the heat transfer fluid between two sorber beds for desorption and adsorption processes. Type T thermocouples (Omega, model #5SRTC-TT-T-36-36) with accuracy of 0.75% of reading and pressure transducers with 0–34.5 kPa operating range (Omega, model #PX309-005AI) and 0.4 kPa accuracy were installed to monitor and record the temperature and pressure variations in each component of the sorption test bed over time. Positive displacement flow meters (FLOMEC, Model # OM015S001-222) with accuracy of 0.5% of reading were installed to measure the flow rate of the heat transfer fluid. The instruments were interfaced with a PC through a data acquisition system and in-house software built in the LabVIEW environment. Experiments were performed continuously until the system reached an oscillatory steady state. The maximum uncertainties in the calculations of COP and SCP were calculated to be 13% and 11%, respectively. More information on the custom-designed capillary-assisted evaporator, uncertainty analysis and the tests can be found in Sharafian et al. (2016).

Fig. 3 shows the sorber bed used in this study, which is an engine oil cooler manufactured by Hayden Automotive (model #1268). The heat exchanger was coated with a composite sorbent consisting of $CaCl_2$, silica gel B150, PVA, and graphite flakes. Details of the sorber bed geometry and heat transfer characteristics are listed in Table 2. This heat exchanger was the closest off-the-shelf heat exchanger to the solution domain of the present model,

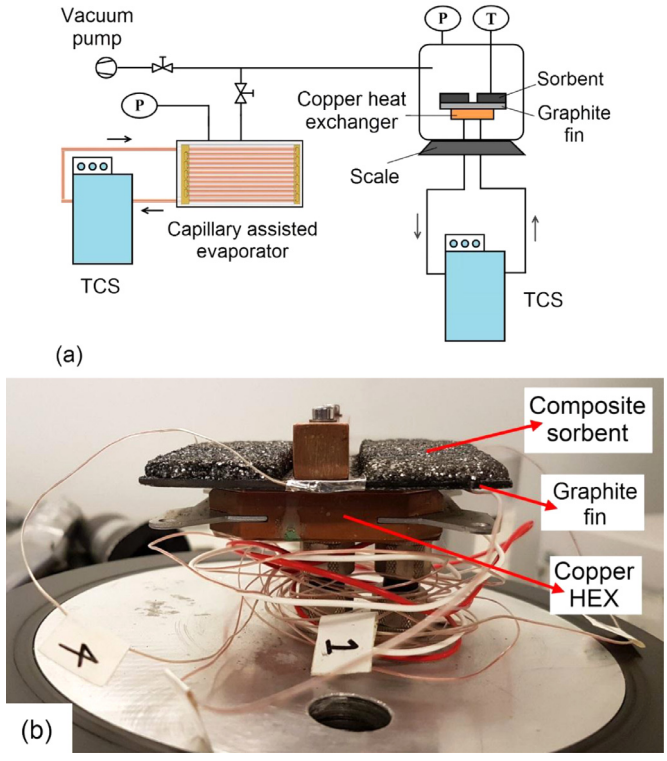

Fig. 4. (a) Schematic diagram of the G-LPJ test bed, and (b) custom-built gravimetric large pressure jump (G-LPJ) test bed.

shown in Fig. 1(a). Therefore, it was used for model validation. We are in the process of design and optimization of sorber beds based on the present model, see Fig. 1(b), which will be presented in our future studies.

4. Experimental study: gravimetric large pressure jump (G-LPJ) test bed

A gravimetric large pressure jump, G-LPJ, test bed was custom-built in our lab to validate the present analytical model results. A schematic diagram of the G-LPJ test bed is shown in Fig. 4(a). Sorbent material, consisting of $CaCl_2$, silica gel B150, PVP-40 and graphite flakes, was coated on graphite sheets and installed in the G-LPJ test bed, see Fig. 4(b). To simulate the operation of a sorption chiller the evaporator temperature was set to 20 °C and condenser temperature to 1 °C while the sample temperature was maintained at 39 °C. The sorber bed was placed on a precision balance (ML4002E, Mettler Toledo) with an accuracy of 0.01 g to measure the mass of the sorbate uptake. More information on G-LPJ tests can be found in Bahrehmand et al. (2018c).

5. Model validation

The graphite flake content in the sorbent, thermophysical properties, geometrical specifications, and SCS cycle parameters used for the baseline case for the parametric study and validation of the present analytical model are listed in Table 2. Thermal diffusivity and specific heat of composite sorbents with different graphite flake contents were measured using a transient plane source (TPS), hot disk thermal constants analyzer, as per ISO 22007-2 (ISO22007-2, 2008) (TPS 2500S, ThermTest Inc., Fredericton, Canada), and averaged between 10% and 40% relative humidity, which is the range of p/p_0 in our tests for sorption air-conditioning applications (T_{des}=90 °C, T_{ads}=T_{cond}=30 °C and T_{evap}=15 °C). Details

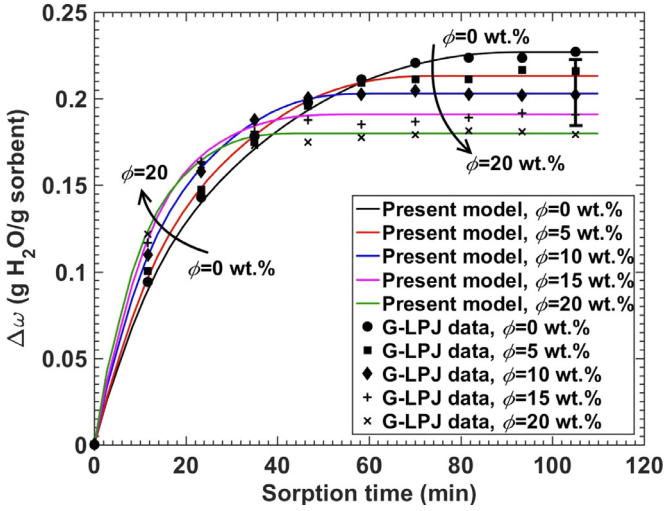

Fig. 5. Comparison of the present analytical model with G-LPJ water uptake data for composite sorbents containing 0–20 wt% graphite flakes, see Table 2 for more details.

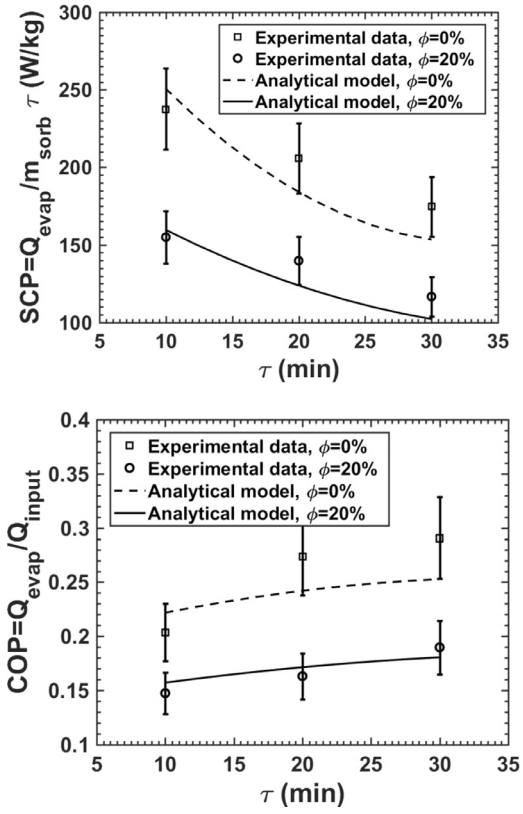

Fig. 6. Comparison between the present analytical model and the experimental data collected from our 2-sorber bed sorption test bed for 0 and 20 wt% graphite flake content in the sorbent composite; see Table 2 for more details.

of TPS testing can be found elsewhere (Fayazmanesh and Bahrami, 2017; Bahrehmand et al., 2018d). Density was calculated by measuring volume and weight. For more information on the operating conditions and the rationale for selection of the listed values please see Bahrehmand et al. (2018a, 2018b).

To validate the model with G-LPJ results, the heat flux in the sorbent boundary condition at $x=0$ in Eq. (5) was set to zero, see Fig. 4(b). Fig. 5 shows the temporal variation of differential water uptake for composite sorbents containing 0–20 wt% natural graphite flakes. The experiments were conducted 5 times to ensure

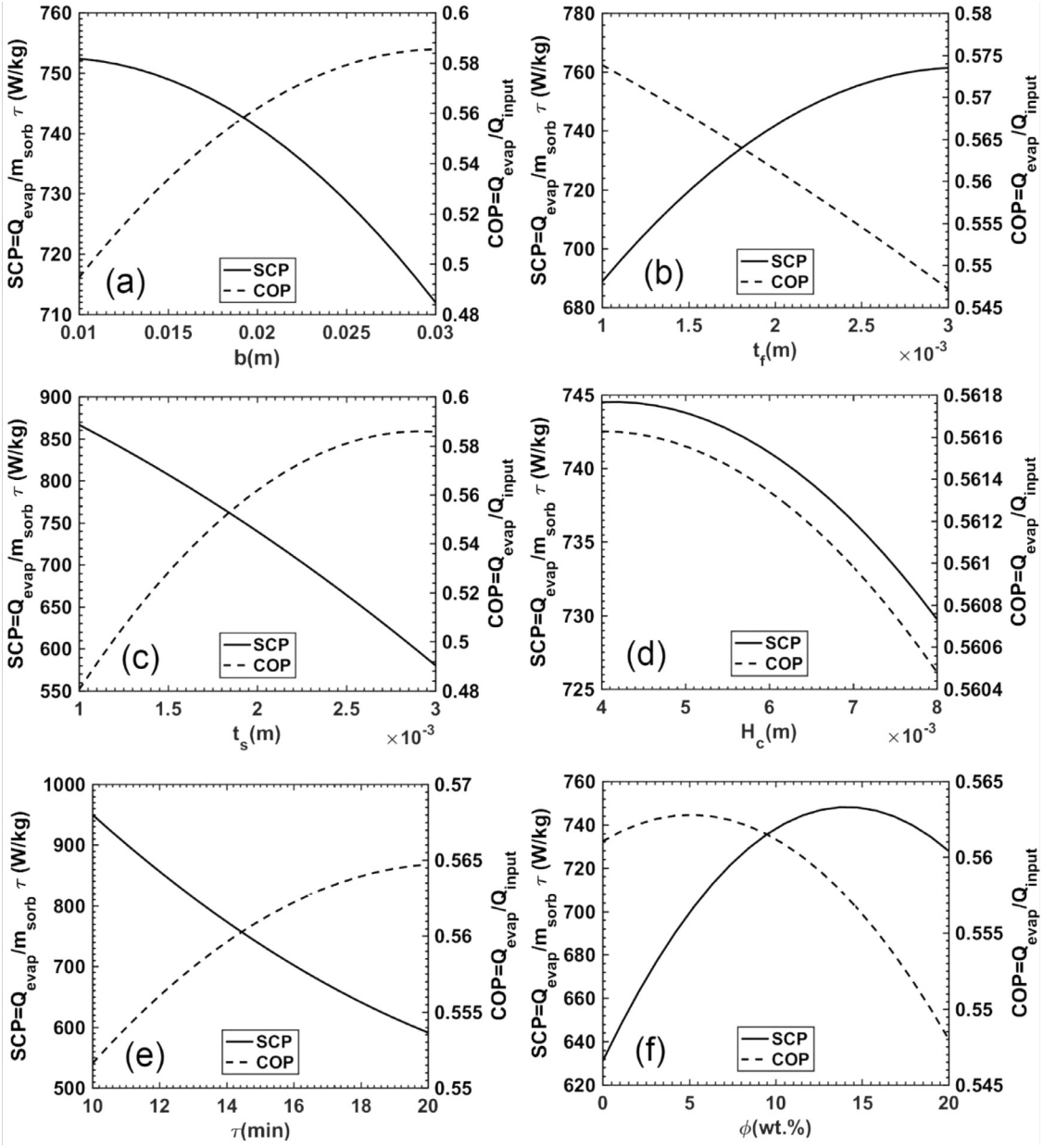

Fig. 7. Parametric study: Variation of SCP and COP with geometrical, heat transfer characteristics of sorber beds and cycle time (a) fin height, (b) fin thickness, (c) sorbent thickness, (d) fluid channel height, (e) cycle time and (f) graphite flake content in the sorbent.

repeatability; the maximum standard deviation was measured at 7%. As shown in Fig. 5, the results predicted by the present analytical model are in a good agreement with the data collected from our G-LPJ test bed. Furthermore, it can be observed that for small sorption times, i.e. less than 20 min, water uptake increases notably by increasing the graphite flake content. The reason is that during this time, the sorption rate, and thus, the heat generation rate is high; consequently, there is a high need for enhanced sorbent thermal diffusivity. Therefore, the uptake increases by increasing the graphite flake even though the sorbent contains less active material. However, over longer time as the sorbent approaches saturation, the sorption rate and heat generation rate decrease, which reduces the need for enhanced thermal diffusivity. As a result, the trend starts to reverse and the sorbent with higher active material starts to have higher uptake. This clearly shows the importance of the graphite flake (conductive additive) content and that it should be optimized based on the cycle time to achieve optimum uptake performance.

Specific cooling power (SCP) is defined as the ratio of evaporative cooling energy to the product of cycle time and dry sorbent mass, Eq. (16). For a sorption cooling system with an ideal evaporator and condenser, SCP represents how fast the heat and mass transfer processes are in the sorber bed.

$$SCP = \frac{Q_{evap}}{m_{sorb}\tau} = \frac{m_{sorb}\int_{ads}\frac{d\omega}{dt}h_{fg}dt}{m_{sorb}\tau} = \frac{\Delta\omega\, h_{fg@T_{evap}}}{\tau} \tag{16}$$

Coefficient of performance (COP) is defined as the ratio of evaporative cooling energy to the input energy, Eq. (17). COP can be increased by: (i) enhancing the heat and mass transfer processes inside the sorber bed, which increases both the evaporative cooling energy and the desorption heat, which overall increases COP,

and (ii) decreasing the thermal inertia of the HEX, which reduces the sensible heat.

$$COP = \frac{Q_{evap}}{Q_{input}} = \frac{Q_{evap}}{Q_{sens} + Q_{des}} = \frac{m_{sorb}\int_{ads}\frac{d\omega}{dt}h_{fg}dt}{\int_{des}\left(\left(m_{sorb}(c_{p,s}+\omega c_{p,w})+m_{HEX}c_{p,HEX}\right)\frac{dT}{dt} - m_{sorb}\frac{d\omega}{dt}h_{ads}\right)dt} \quad (17)$$

Fin height ranges from 1.08 to 1.40 cm around the tubes in the heat exchanger shown in Fig. 3. Over this range of fin height, the maximum change in SCP and COP is 0.7% and 3%, respectively, compared to the SCP and COP obtained using the average fin height used in this study, i.e., 1.24 cm, listed in Table 2. Therefore, the average fin height is used for the model validation. Fig. 6 shows the comparison between the SCP and COP calculated using the proposed analytical model against the data measured using our two-sorber bed sorption test bed. As seen in Fig. 6, the present model is in a general good agreement with the experimental data.

6. Parametric study and performance evaluation

A comprehensive parametric study is performed in which a sorber bed was considered as a baseline case (Table 2) and each parameter is varied systematically – over an arbitrarily chosen range – while all others kept constant. Fig. 7 shows the variation of SCP and COP with fin height, fin thickness, sorbent thickness, fluid channel height, graphite flake content in the sorbent, and the cycle time. The following can be observed:

(a) By increasing the fin height, SCP decreases as the heat transfer resistance along the fin increases. Nonetheless, by increasing the fin height, COP increases because the evaporative cooling energy, numerator in Eq. (17), increases more than the total input energy, denominator in Eq. (17).
(b) By increasing the fin thickness, SCP increases as the heat transfer along the fin enhances due to more cross-section area. However, by increasing the fin thickness, COP reduces because the HEX thermal inertia increases.
(c) By increasing the sorbent thickness, SCP decreases as the sorbent heat transfer resistance increases. Nevertheless, by increasing the sorbent thickness, COP increases because the relative thermal inertia of HEX to sorbent decreases.
(d) By reducing the fluid channel height, both SCP and COP increase as the convective heat transfer coefficient of the heat transfer fluid increases.
(e) Sorption rate is high at the early stages of sorption and decreases rather rapidly as the sorbent approaches saturation. Consequently, by decreasing the cycle time, SCP increases as the sorption rate, and thus, the evaporative cooling power increases. However, by reducing the cycle time, COP decreases because more energy is needed for the sensible heat of the sorber bed HEX thermal inertia compared to the desorption heat.
(f) Adding graphite flakes to the sorbent enhances its thermal diffusivity notably (up to 500%, Bahrehmand et al., 2018c) and reduces the active sorbent material. It is key to select an optimum amount of graphite flake additive, which depends on the sorber bed geometry, cycle time, and heat transfer characteristics. If the main thermal resistance in the sorber bed HEX is the sorbent, by increasing the graphite flake content, SCP increases to the point that the sorbent thermal resistance becomes comparable to the thermal resistances of HEX or heat transfer fluid. After this point, SCP starts to decrease by any further increase in the graphite flake content because the active sorbent material reduces. This trend can be seen in Fig. 7(f). As for COP, the optimum graphite flake content is smaller than that of the SCP as the effect of active sorbent material on COP is more than the heat transfer. On the other hand, if the sorbent thermal resistance is not the main thermal resistance in the sorber bed HEX, adding graphite flakes does not increase the performance as the heat transfer is limited by other thermal resistances in the sorber bed, e.g. HEX and/or heat transfer fluid. Therefore, adding graphite flakes reduces the performance since it decreases the active sorbent material, see Fig. 8. In this case, the enhanced sorbent thermal diffusivity does not increase the total heat transfer noticeably as the heat transfer is limited by the thin fin, i.e. 0.1 mm thickness.

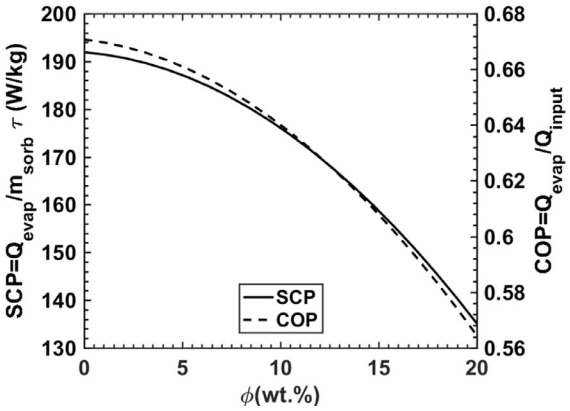

Fig. 8. Variation of SCP and COP with graphite flake content in the sorbent for $b = 2$ cm, $t_s = 1$ mm, $t_f = 0.1$ mm, $H_c = 6$ mm and $\tau = 15$ min.

It is evident that the geometrical and heat transfer characteristics of the sorbent, heat exchanger and heat transfer fluid should be optimized simultaneously because even one large resistance in the heat transfer between the sorbent and heat transfer fluid through the heat exchanger can limit the performance.

7. Conclusions

A novel accurate transient 2-D analytical closed-form solution was developed that considers all salient design parameters, including: HEX 2-D geometry, thermophysical and sorbent material properties, and thermal contact resistance of sorber beds. The model was successfully validated with the experimental data collected from our gravimetric large pressure jump test bed and two-sorber bed sorption test bed. The present analytical model provides a reliable and easy-to-use design and optimization tool for finned tube sorber bed heat exchangers of SCS. The solution methodology can be applied to other sorber bed types, such as radial and annular finned tubes and plate sorber beds. It was shown that the sorber bed geometry and heat transfer characteristics should be optimized simultaneously because if even one thermal resistance remains large inside the sorber bed, sorbent, HEX and/or heat transfer fluid, it can limit the heat transfer and overall performance of SCS.

Moreover, it was indicated that the geometrical and heat transfer characteristics of sorber beds, i.e. fin height, fin thickness, sorbent thickness, fluid channel height, graphite flake content in the sorbent, and cycle time, have counteracting effects on SCP and COP. Hence, multi-objective optimization of sorber beds should be conducted considering all these parameters to find an optimal design for SCP and COP, and therefore, increase the SCS performance.

Acknowledgment

The first author thanks the LAEC member, Dr. Claire McCague, postdoctoral fellow, for her help with the experiments. The authors gratefully acknowledge the financial support of the Natural Sciences and Engineering Research Council of Canada (NSERC) through the Automotive Partnership Canada Grant no. APCPJ 401826-10.

Appendix A

The following non-dimensional variables are defined.

$$\theta = \frac{T - T_{fluid}}{T_0 - T_{fluid}} \qquad \xi = \frac{y}{t_s + t_f} \qquad \eta = \frac{x}{b}$$

$$Bi_s = \frac{b}{R_s k_s} \qquad Bi_f = \frac{b}{R_f k_f} \qquad \kappa = \frac{k_s}{k_y}$$

$$\Lambda = \frac{t_s + t_f}{k_y TCRA} \qquad Fo = \frac{t\alpha_x}{b^2} \qquad \delta = \frac{b}{t_s + t_f}$$

$$\mu_y{}^2 = \frac{\alpha_y}{\alpha_x} \qquad \mu_s{}^2 = \frac{\alpha_s}{\alpha_x} \qquad \delta_f = \frac{t_f}{t_s + t_f}$$

where, θ is the dimensionless temperature, the Fourier number, Fo, is the dimensionless time, ξ and η are the dimensionless Cartesian coordinates. Using the aforementioned dimensionless variables, the dimensionless energy equation can be obtained as follows.

$$\frac{\partial \theta_i}{\partial Fo} = \mu_{i,\eta}{}^2 \frac{\partial^2 \theta_i}{\partial \eta^2} + \left(\mu_{i,\xi}\delta\right)^2 \frac{\partial^2 \theta_i}{\partial \xi^2} + g_i(Fo)$$
$$\theta_i(\eta, \xi, Fo)$$
$$i = s, f \tag{A1}$$

where

$$g_i(Fo) = \begin{cases} \frac{(1-\varepsilon)h_{ads}}{c_{p,s}(T_0 - T_{fluid})} \frac{d\omega}{dFo}, & i = s \\ 0, & i = f \end{cases} \tag{A2}$$

$$\mu_{i,\eta} = \begin{cases} 1, & i = f \\ \mu_s, & i = s \end{cases} \tag{A3}$$

$$\mu_{i,\xi} = \begin{cases} \mu_y, & i = f \\ \mu_s, & i = s \end{cases} \tag{A4}$$

Water uptake can be modeled in terms of the operating conditions, i.e. pressure and temperature of the sorber bed. A linear relationship is obtained between the water uptake and sorbent temperature for each pressure during the isobaric sorption and desorption processes. Detailed explanation is presented in Appendix B.

The dimensionless boundary conditions are:

$$\frac{\partial \theta_s(0, \xi, Fo)}{\partial \eta} - Bi_s \theta_s(0, \xi, Fo) = 0 \tag{A5}$$

$$\frac{\partial \theta_f(0, \xi, Fo)}{\partial \eta} - Bi_f \theta_f(0, \xi, Fo) = 0 \tag{A6}$$

$$\frac{\partial \theta_s(\eta, 1, Fo)}{\partial \xi} = 0 \tag{A7}$$

$$\frac{\partial \theta(1, \xi, Fo)}{\partial \eta} = 0 \tag{A8}$$

$$\frac{\partial \theta_f(\eta, 0, Fo)}{\partial \xi} = 0 \tag{A9}$$

$$\frac{\partial \theta_f(\eta, \delta_f, Fo)}{\partial \xi} = \kappa \frac{\partial \theta_s(\eta, \delta_f, Fo)}{\partial \xi} \tag{A10}$$

$$-\frac{\partial \theta_f(\eta, \delta_f, Fo)}{\partial \xi} = \Lambda\left(\theta_f(\eta, \delta_f, Fo) - \theta_s(\eta, \delta_f, Fo)\right) \tag{A11}$$

The dimensionless energy equation, Eqs. (A1)–(A11), is solved using Eigenfunction Expansion Method. The closed-form of the dimensionless temperature is as follows.

$$\theta(\eta, \xi, Fo) = \sum_{n=1}^{\infty} \sum_{m=1}^{\infty} X_n(\eta) \psi_{nm}(\xi) \Gamma_{nm}(Fo) \tag{A12}$$

Based on Eqs. (A1)–(A12), the following eigen-value problem can be established in η direction (Mikhailov and Ozisik, 1986).

$$X'' + \gamma^2 X = 0 \tag{A13}$$

$$X' - Bi\, X = 0 \text{ at } \eta = 0 \tag{A14}$$

$$X' = 0 \text{ at } \eta = 1 \tag{A15}$$

The following transcendental equation is obtained to evaluate the eigenvalues.

$$\gamma \tan(\gamma) = Bi \tag{A16}$$

The eigenfunction associated with each eigenvalue are given as follows.

$$X = \cos(\gamma\eta) + \tan(\gamma)\sin(\gamma\eta) \tag{A17}$$

Moreover, the eigen-value problem in ξ direction can be established as follows.

$$\frac{d^2\psi}{d\xi^2} + \omega_k^2 \psi = 0 \tag{A18}$$

$$\frac{d\psi}{d\xi}\Big|_{\xi=0,1} = 0 \tag{A19}$$

where,

$$\omega_k{}^2 = \frac{\lambda r_k - q_k}{p_k}, \; k = s, f \tag{A20}$$

$$r_s = \frac{\left((\rho c_p)_s - \left(\rho h_{ads} m'\right)_s\right) k_x}{(\rho c_p)_f \delta^2} \tag{A21}$$

$$r_f = \frac{k_x}{\delta^2} \tag{A22}$$

$$q_k = \left(\mu_{k,\eta}\gamma\right)^2 r_k \tag{A23}$$

$$p_f = k_y \tag{A24}$$

$$p_s = k_s \tag{A25}$$

This is a singular eigenvalue problem due to non-continuous p, r and q. Also, $\omega_k{}^2$ can be positive, negative or zero depending on the thermophysical properties and geometrical characteristics of the sorbent and the fin as well as the eigenvalue in η direction (γ). Thus, the eigenvalue problem does not have a simple solution with eigenfunction and transcendental equation. The present paper follows the solution proposed by Mikhailov and Vulchanov (1983). First, the eigenvalue problem is approximated by uniformly dividing the slabs (sorbent and fin) into n–1 intervals (n is an arbitrary number at first). The finer the division of the intervals,

the more accurate the approximation. The new eigenvalue problem with boundary conditions are as follows.

$$\frac{d^2\psi}{d\xi^2} + \omega_k^2\psi = 0 \tag{A26}$$

$$\frac{d\psi}{d\xi}\Big|_{\xi=0} = 0 \tag{A27}$$

$$\psi_k = \psi_{k+1},\ k = 1, 2, ..., n-2 \tag{A28}$$

$$p_k\frac{d\psi_k}{d\xi} = p_{k+1}\frac{d\psi_{k+1}}{d\xi},\ k = 1, 2, ..., n-2 \tag{A29}$$

$$\frac{d\psi}{d\xi}\Big|_{\xi=1} = 0 \tag{A30}$$

$$l_k = \xi_{k+1} - \xi_k \tag{A31}$$

TCR at the interface between the sorbent and the fin is taken into account as an additional imaginary layer as follows.

$$\frac{d^2\psi}{d\xi^2} + \omega_k^2\psi = 0 \tag{A32}$$

$$\omega_k = 0 \tag{A33}$$

$$p_k\frac{d\psi_k}{d\xi} = \frac{t_s + t_f}{TCR\cdot A}(\psi_{k+1} - \psi_k) \tag{A34}$$

Hence, the thermal conductivity of this layer must satisfy the following equation for an arbitrary length of l_k.

$$p_k = \frac{\left(t_s + t_f\right) l_k}{TCR\cdot A} \tag{A35}$$

The following eigenfunctions can be acquired for each interval ($\xi_k < \xi < \xi_{k+1}$).

$$\psi_k(\xi) = \psi_k(\xi_k)\frac{\sin\left(\omega_k(\xi_{k+1} - \xi)\right)}{\sin\left(\omega_k l_k\right)} + \psi_k(\xi_{k+1})\frac{\sin\left(\omega_k(\xi - \xi_k)\right)}{\sin\left(\omega_k l_k\right)},\ {\omega_k}^2 > 0 \tag{A36}$$

$$\psi_k(\xi) = \psi_k(\xi_k)\frac{(\xi_{k+1} - \xi)}{l_k} + \psi_k(\xi_{k+1})\frac{(\xi - \xi_k)}{l_k},\ {\omega_k}^2 = 0 \tag{A37}$$

$$\psi_k(\xi) = \psi_k(\xi_k)\frac{\sinh\left(\omega_k^*(\xi_{k+1} - \xi)\right)}{\sinh\left(\omega_k^* l_k\right)} + \psi_k(\xi_{k+1})\frac{\sinh\left(\omega_k^*(\xi - \xi_k)\right)}{\sinh\left(\omega_k^* l_k\right)},\ {\omega_k}^2 < 0$$

$$\omega_k^* = \sqrt{\mathrm{abs}\left({\omega_k}^2\right)} \tag{A38}$$

By substituting the aforementioned eigenfunctions into the boundary conditions ((A27)–(A30)), the following equations can be obtained to calculate the eigenfunctions for each interval.

$$\begin{aligned} &A_1\psi_0 - B_1\psi_1 = 0 \\ &-B_k\psi_{k-1} + (A_k + A_{k+1})\psi_k - B_{k+1}\psi_{k+1} = 0,\ k = 1, 2, ..., n-1 \\ &-B_n\psi_{n-1} + A_n\psi_n = 0 \end{aligned} \tag{A39}$$

where,

$$\begin{aligned} B_k &= \frac{p_k\omega_k}{\sin\left(\omega_k l_k\right)},\ {\omega_k}^2 > 0 \\ B_k &= \frac{p_k}{l_k},\ {\omega_k}^2 = 0 \\ B_k &= \frac{p_k\omega_k^*}{\sinh\left(\omega_k^* l_k\right)},\ {\omega_k}^2 < 0 \end{aligned} \tag{A40}$$

$$\begin{aligned} A_k &= B_k\cos\left(\omega_k l_k\right),\ {\omega_k}^2 > 0 \\ A_k &= B_k,\ {\omega_k}^2 = 0 \\ A_k &= B_k\cosh\left(\omega_k^* l_k\right),\ {\omega_k}^2 < 0 \end{aligned} \tag{A41}$$

(A39) forms a linear system of $(n+1)$ homogeneous equations for determination of the eigenfunctions as follows.

$$[K]\{\psi\} = 0 \tag{A42}$$

By equating the determinant of coefficient matrix $[K]$ to zero, the transcendental equation is acquired to evaluate the eigenvalues.

$$\det([K]) = 0 \tag{A43}$$

The eigenvalues are calculated using the algorithm proposed by Mikhailov and Vulchanov which is based on sign-count method (Mikhailov and Vulchanov, 1983). The accuracy in obtaining the eigenvalues is set to 0.001.

Subsequently, the eigenfunctions are calculated as follows.

$$\psi_0 = -1 \tag{A44}$$

$$\psi_1 = -A_1/B_1 \tag{A45}$$

$$\psi_{k+1} = ((A_k + A_{k+1})\psi_k - B_k\psi_{k-1})/B_{k+1},\ k = 1,\ 2,\ ...,\ n-1 \tag{A46}$$

Afterwards, the accuracy of the eigenfunctions is calculated for the last interval.

$$\mathrm{abs}(-B_n\psi_{n-1} + A_n\psi_n) \le \varepsilon_{global},\ \varepsilon_{global} \cong \varepsilon_{\max}\cdot n \tag{A47}$$

where, the accuracy is set to 1e-8 in the present study. If this accuracy requirement is not satisfied, then the intervals are refined based on the algorithm proposed by Mikhailov and Vulchanov (1983) until it is satisfied.

Now that the eigenfunctions in η and ξ directions are calculated, the last step is to obtain Gamma function (Γ) which represents the time variation of θ.

Every time-dependent function can be expanded in the form of infinite series of products of the eigenfunctions in η and ξ directions.

$$g_i(Fo) = \sum_{n=1}^{\infty}\sum_{m=1}^{\infty} g_{nm}^*(Fo)X_n(\eta)\psi_{nm}(\xi) \tag{A48}$$

where, using the orthogonal property of the Eigenfunctions

$$g_{nm}^*(Fo) = \frac{g_i(Fo)\int_0^1 X d\eta\left(\sum_{k=1}^{n} r_k\int_{\xi_k}^{\xi_{k+1}}\psi_k d\xi\right)}{\int_0^1 X^2 d\eta\left(\sum_{k=1}^{n} r_k\int_{\xi_k}^{\xi_{k+1}}{\psi_k}^2 d\xi\right)} \tag{A49}$$

By substituting Eqs. (A12) and (A48) into Eq. (A1), an ordinary differential equation for Gamma function can be acquired as follows.

$$\frac{d\Gamma}{dFo} = g^*_{nm}(Fo) - \lambda\Gamma \tag{A50}$$

Finally, Gamma function is calculated by (A51).

$$\Gamma = e^{-\lambda Fo}\left(C_{nm} + \int_{Fo'=0}^{Fo} g^*_{nm}(Fo')e^{\lambda Fo'}dFo'\right) \tag{A51}$$

where,

$$C_{nm} = \frac{\int_0^1 X d\eta \left(\sum_{k=1}^{n} r_k \int_{\xi_k}^{\xi_{k+1}} \psi_k d\xi\right)}{\int_0^1 X^2 d\eta \left(\sum_{k=1}^{n} r_k \int_{\xi_k}^{\xi_{k+1}} {\psi_k}^2 d\xi\right)} \tag{A52}$$

Appendix B

Sorber beds go through two isosteric processes, i.e. cooling and heating, during which the water uptake remains constant because the valves to the evaporator and condenser are closed. Each isosteric process is followed by an isobaric process when the sorber bed is connected to the evaporator or condenser, and sorption or desorption occurs. During isobaric processes, the pressure of the sorber bed chamber is almost equal to that of evaporator or condenser and assumed constant. Fig. B1 shows the variation of water uptake versus sorbent temperature for each isobaric process obtained from gravimetric large pressure jump (G-LPJ) test bed with T_{evap}=20 °C and T_{cond}=1 °C, see Bahrehmand et al. (2018a, 2018b). It can be seen that the equilibrium water uptake collected from Thermogravimetric analyzer (TGA) is in a good agreement with the data measured using our custom-built G-LPJ test bed. More information on TGA measurements can be found elsewhere (Bahrehmand et al., 2018c). Therefore, for each isobaric process, whose pressure is the saturation pressure at condenser or evaporator temperature, a relationship can be acquired between the water uptake and sorbent temperature. For simplicity in the 2-D analytical model, this relationship is approximated with a line. Fig. B2 shows the isobaric processes acquired from TGA for pressure values corresponding to T_{evap}=15 °C and T_{cond}=30 °C for large temperature jump (LTJ) tests.

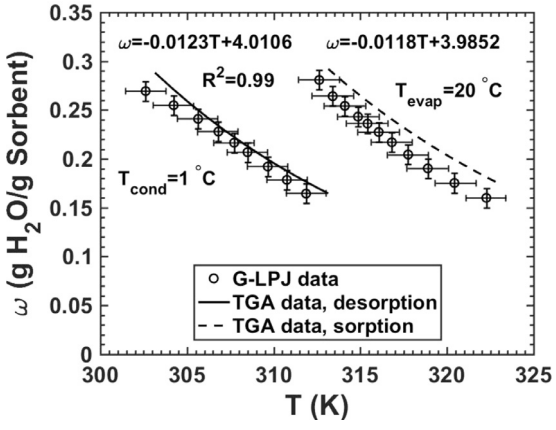

Fig. B1. Variation of water uptake versus sorbent temperature for large pressure jump tests.

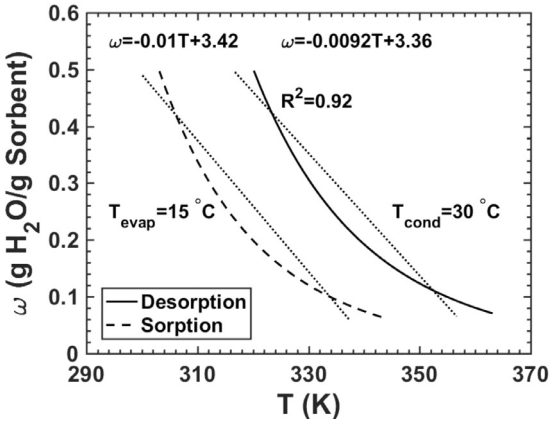

Fig. B2. Variation of water uptake versus sorbent temperature for large temperature jump tests.

References

Ahmed, R., Al-Dadah, R., 2012. Physical and operating conditions effects on silica gel/water adsorption chiller performance. Appl. Energy 89, 142–149.

Askalany, A.A., Salem, M., Ismael, I.M., Ali, A.H.H., Morsy, M.G., Saha, B.B., 2013. An overview on adsorption pairs for cooling. Renew. Sustain. Energy Rev. 19, 565–572.

Bahrehmand, H., Khajehpour, M., Bahrami, M., 2018c. Finding optimal conductive additive content to enhance the performance of coated sorption beds: an experimental study. Appl. Therm. Eng. 143, 308–315.

Bahrehmand, H., Ahmadi, M., Bahrami, M., 2018a. Analytical modeling of oscillatory heat transfer in coated sorption beds. Int. J. Heat Mass Transf. 121, 1–9.

Bahrehmand, H., Ahmadi, M., Bahrami, M., 2018b. Oscillatory heat transfer in coated sorber beds: an analytical solution. Int. J. Refrig. doi:10.1016/j.ijrefrig.2018.05.006.

Bahrehmand, H., Khajehpour, M., Bahrami, M., 2018d. Finding optimal conductive additive content to enhance the performance of coated sorption beds: an experimental study. Appl. Therm. Eng. 143, 308–315.

Biswas, P., Singh, S., 2017. Orthogonal eigenfunction expansion method for one-dimensional dual-phase lag heat conduction problem with time-dependent boundary conditions. J. Heat Transf. 140 (3), 034501.

Building Energy Data Book. U.S. Department of Energy, by D&R International, Ltd., under contract to Pacific Northwest National Laboratory, 2012.

Çağlar, A., 2016. The effect of fin design parameters on the heat transfer enhancement in the adsorbent bed of a thermal wave cycle. Appl. Therm. Eng. 104, 386–393.

El Fadar, A., 2015. Thermal behavior and performance assessment of a solar adsorption cooling system with finned adsorber. Energy 83, 674–684.

Fakoor-Pakdaman, M., Ahmadi, M., Bagheri, F., Bahrami, M., 2015. Optimal time–varying heat transfer in multilayered packages with arbitrary heat generations and contact resistance. J. Heat Transf. 137 (8), 081401.

Fayazmanesh, K., Bahrami, M., 2017. Consolidated Composite Adsorbent Containing Graphite Flake for Sorption Cooling Systems.

Gnielinski, V., 1976. New equations for heat and mass transfer in turbulent pipe and channel flow. Int. Chem. Eng. 16 (2), 359–368.

Golparvar, B., Niazmand, H., Sharafian, A., Ahmadian Hosseini, A., 2018. Optimum fin spacing of finned tube adsorber bed heat exchangers in an exhaust gas-driven adsorption cooling system. Appl. Energy 232, 504–516.

Henninger, S., Schicktanz, M., Hugenell, P., Sievers, H., Henning, H., 2012. Evaluation of methanol adsorption on activated carbons for thermally driven chillers, part I: thermophysical characterisation. Int. J. Refrig. 35, 543–553.

Hong, S.W., Ahn, S.H., Kwon, O.K., Chung, J.D., 2015. Optimization of a fin-tube type adsorption chiller by design of experiment. Int. J. Refrig. 49, 49–56.

https://www.nrcan.gc.ca 2018.

Hu, E.J., Zhu, D., Sang, X., Wang, L., Tan, Y., 1997. Enhancement of thermal conductivity by using polymer-zeolite in solid adsorption heat pumps. J. Heat Transf. 1, 1991–1993.

ISO22007-2, "Plastics-determination of Thermal Conductivity and Thermal Diffusivity-Part 2: Transient Plane Heat Source (Hot Disc) Method." 2008.

Jeric, M.Z., Nottage, H.B., 1967. Coupled periodic heat and mass transfer through a permeable slab with vapor adsorption. J. Heat Transf. 89 (1), 44–52.

Julius, S., Leizeronok, B., Cukurel, B., 2017. Nonhomogeneous dual-phase-lag heat conduction problem: analytical solution and select case studies. J. Heat Transf. 140 (3), 031301.

Li, J., Kubota, M., Watanabe, F., Kobayashi, N., Hasatani, M., 2004. Optimal design of a fin-type silica gel tube module in the silica gel/water adsorption heat pump. J. Chem. Eng. Jpn. 37 (4), 551–557.

Mahdavikhah, M., Niazmand, H., 2013. Effects of plate finned heat exchanger parameters on the adsorption chiller performance. Appl. Therm. Eng. 50, 939–949.

Mikhailov, M.D., Ozisik, M.N., 1986. Transient conduction in a three-dimensional composite slab. Int. J. Heat Mass Transf. 29, 340–342.

Mikhailov, M.D., Vulchanov, N.L., 1983. Computational procedure for Sturm–Liouville problems. J. Comput. Phys. 50, 323–336.
Moghadam, A.J., 2015. Exact solution of electroviscous flow and heat transfer in a semi-annular microcapillary. J. Heat Transf. 138 (1), 011702.
Mohammadzadeh Kowsari, M., Niazmand, H., Tokarev, M.M., 2018. Bed configuration effects on the finned flat-tube adsorption heat exchanger performance: numerical modeling and experimental validation. Appl. Energy 213, 540–554.
Mohammed, R.H., Mesalhy, O., Elsayed, M.L., Chow, L.C., 2017. Novel compact bed design for adsorption cooling systems: parametric numerical study. Int. J. Refrig. 80, 238–251.
Niazmand, H., Dabzadeh, I., 2012. Numerical simulation of heat and mass transfer in adsorbent beds with annular fins. Int. J. Refrig. 35, 581–593.
Niazmand, H., Talebian, H., Mahdavikhah, M., 2012. Bed geometrical specifications effects on the performance of silica/water adsorption chillers effets des spécifications géométriques du lit sur la performance des refroidisseurs à adsorption au gel de silice/eau. Int. J. Refrig. 35 (8), 2261–2274.
Pan, Q.W., Wang, R.Z., Wang, L.W., Liu, D., 2016. Design and experimental study of a silica gel-water adsorption chiller with modular adsorbers. Int. J. Refrig. 67, 336–344.
Pan, Q.W., Wang, R.Z., 2017a. Study on boundary conditions of adsorption heat pump systems using different working pairs for heating application. Energy Convers. Manag. 154, 322–335.
Pan, Q., Wang, R., Vorayos, N., Kiatsiriroat, T., 2018. A novel adsorption heat pump cycle: cascaded mass recovery cycle. Int. J. Refrig. 95, 21–27.
Pan, Q.W., Wang, R.Z., 2017b. Experimental study on operating features of heat and mass recovery processes in adsorption refrigeration. Energy 135, 361–369.
Pan, Q.W., Wang, R.Z., 2018. Study on operation strategy of a silica gel-water adsorption chiller in solar cooling application. Sol. Energy 172, 24–31.
Pridasawas, W., 2006. Solar-driven Refrigeration Systems with Focus on the Ejector Cycle. Department of Energy Technology, Royal Institute of Technology, p. 2006 no. 06/55.
Rezk, A., Al-Dadah, R.K., Mahmoud, S., Elsayed, A., 2013. Effects of contact resistance and metal additives in finned-tube adsorbent beds on the performance of silica gel/water adsorption chiller. Appl. Therm. Eng. 53 (2), 278–284.
Rogala, Z., 2017. Adsorption chiller using flat-tube adsorbers – performance assessment and optimization. Appl. Therm. Eng. 121, 431–442.
Saha, B., El-Sharkawy, I., Chakraborty, A., Koyama, S., 2007. Study on an activated carbon fiber-ethanol adsorption chiller: part I – system description and modelling. Int. J. Refrig. 30, 86–95.
Sharafian, A., McCague, C., Bahrami, M., 2015. Impact of fin spacing on temperature distribution in adsorption cooling system for vehicle A/C applications. Int. J. Refrig. 51, 135–143.
Sharafian, A., Bahrami, M., 2014. Assessment of adsorber bed designs in waste-heat driven adsorption cooling systems for vehicle air conditioning and refrigeration. Renew. Sustain. Energy Rev. 30, 440–451.
Sharafian, A., Fayazmanesh, K., Mccague, C., Bahrami, M., 2014. Thermal conductivity and contact resistance of mesoporous silica gel adsorbents bound with polyvinylpyrrolidone in contact with a metallic substrate for adsorption cooling system applications. Int. J. Heat Mass Transf. 79, 64–71.
Sharafian, A., Nemati Mehr, S.M., Thimmaiah, P.C., Huttema, W., Bahrami, M., 2016. Effects of adsorbent mass and number of adsorber beds on the performance of a waste heat-driven adsorption cooling system for vehicle air conditioning applications. Energy 112, 481–493.
Singh, S., Jain, P.K., Rizwan-uddin, 2016. Analytical solution for three-dimensional, unsteady heat conduction in a multilayer sphere. J. Heat Transf. 138 (10), 101301.
Solmus, I., Andrew, D., Rees, S., Yamalı, C., Baker, D., 2012. A two-energy equation model for dynamic heat and mass transfer in an adsorbent bed using silica gel/water pair. Int. J. Heat Mass Transf. 55, 5275–5288.
Tamainot-Telto, Z., Metcalf, S.J., Critoph, R.E., Zhong, Y., Thorpe, R., 2009. Carbon–ammonia pairs for adsorption refrigeration applications : ice making, air conditioning and heat pumping les couples charbon actif-ammoniac pour les applications ' adsorption : fabrication de glace, frigorifiques a 'chaleur conditionnement d'. Int. J. Refrig. 32 (6), 1212–1229.
Verde, M., Harby, K., Corberán, J.M., 2017. Optimization of thermal design and geometrical parameters of a flat tube-fin adsorbent bed for automobile air-conditioning. Appl. Therm. Eng. 111, 489–502.
Wakao, N., Kaguei, S., 1982. Heat and Mass Transfer in Packed Beds, vol. 23.
Weng, C., Chen, C., Fin, C.S., 1983. Transient response of a composite straight fin. J. Heat Transf. 105, 307–311 2014.
Wu, W., Zhang, H., Sun, D., 2009. Mathematical simulation and experimental study of a modified zeolite 13X–water adsorption refrigeration module. Appl. Therm. Eng. 29, 645–651.
Zhao, Y., Hu, E., Blazewicz, A., 2012. Dynamic modelling of an activated carbon–methanol adsorption refrigeration tube with considerations of interfacial convection and transient pressure process. Appl. Energy 95, 276–284.